Acta Crystallographica Section D
Biological Crystallography
ISSN 0907-4449

Isomerization mechanism of aspartate to isoaspartate implied by structures of *Ustilago sphaerogena* ribonuclease U2 complexed with adenosine 3′-monophosphate

Shuji Noguchi

Graduate School of Pharmaceutical Sciences, The University of Tokyo, Hongo, Bunkyo-ku, Tokyo 113-0033, Japan

Correspondence e-mail: snoguchi@mol.f.u-tokyo.ac.jp

Received 12 April 2010
Accepted 25 May 2010

PDB References: ribonuclease U2 complexed with adenosine 3′-monophosphate, 3agn; 3ago.

Aspartates in proteins are isomerized non-enzymatically to isoaspartate *via* succinimide *in vitro* and *in vivo*. In order to elucidate the mechanism of isoaspartate formation within the Asp45-Glu46 sequence of *Ustilago sphaerogena* ribonuclease U2 based on three-dimensional structure, crystal structures of ribonuclease U2 complexed with adenosine 3′-monophosphate have been solved at 0.96 and 0.99 Å resolution. The crystal structures revealed that the C^{γ} atom of Asp45 is located just beside the main-chain N atom of Glu46 and that the conformation which is suitable for succinimide formation is stabilized by a hydrogen-bond network mediated by water molecules 190, 219 and 220. These water molecules are suggested to promote the formation of isoaspartate *via* succinimide: in the succinimide-formation reaction water 219 receives a proton from the N atom of Glu46 as a general base and waters 190 and 220 stabilize the tetrahedral intermediate, and in the succinimide-hydrolysis reaction water 219 provides a proton for the N atom of Glu46 as a general acid. The purine-base recognition scheme of ribonuclease U2 is also discussed.

1. Introduction

Proteins are damaged by various chemical post-translational modifications such as oxidation, methylation, isomerization of aspartate and deamidation of asparagine. Isomerization of Asp and deamidation of Asn proceed non-enzymatically and result in the formation of isoaspartate (isoAsp) *via* succinimide (Fig. 1). A number of proteins containing isoAsp have been reported *in vivo* and *in vitro*: for example, monoclonal antibodies (Cacia *et al.*, 1996; Dick *et al.*, 2009), Bcl-x_L (Aritomi *et al.*, 1997), β-amyloid peptide from Alzheimer's disease brain (Roher *et al.*, 1993), calmodulin (Potter *et al.*, 1993), interleukin-11 (Zhang *et al.*, 2002), αA-crystallin (Fujii, Ishibashi *et al.*, 1994), αB-crystallin (Fujii, Satoh *et al.*, 1994) and prion protein (Weber *et al.*, 1998). In the case of αB-crystallin, protein with isoAsp accumulates in the lens of aged humans, suggesting that isoAsp formation might be involved in the aging process. *In vivo*, isoAsps are thought to be repaired by protein isoaspartyl methyltransferase (PIMT; Clarke, 1993). Proteins with isoAsp are known to accumulate in the tissues of PIMT-deficient mice (Kim *et al.*, 1997). The

Table 1
X-ray diffraction data-collection and refinement summary.

Values in parentheses are for the highest resolution shell.

Crystal type	VIII	IX
Crystal parameters		
Space group	$P2_1$	$P2_1$
Unit-cell parameters (Å, °)	a = 37.880, b = 39.789, c = 35.884, β = 114.991	a = 34.586, b = 39.425, c = 31.646, β = 109.979
Data collection		
Wavelength (Å)	0.978	0.978
Resolution range (Å)	34.3–0.960 (0.984–0.960)	34.3–0.990 (1.02–0.990)
No. of observed reflections	857736	364820
No. of unique reflections	58543	39756
Completeness (%)	98.9 (86.3)	96.2 (92.4)
Multiplicity	14.7 (5.0)	9.2 (6.7)
Mean $I/\sigma(I)$	72.2 (7.4)	58.0 (6.6)
R_{merge} (%)	5.2 (29.5)	6.1 (43.3)
Refinement statistics		
R_{work}/R_{free} (%)	11.7/12.7 (23.8/25.2)	15.0/16.2 (38.2/37.4)
Protein molecules per ASU†	1	1
No. of atoms (non-H)		
Protein	919	894
Ligand/ion	25	28
Water	166	100
R.m.s. deviations		
Bond lengths (Å)	0.012	0.014
Bond angles (°)	2.405	1.900
ESU‡ (Å)	0.009	0.016
Average B factors (Å^2)		
Protein	5.25	8.52
Ligand/ion	4.46	7.32
Water	13.6	15.5
Ramachandran statistics		
Favoured (%)	98.2	96.4
Allowed (%)	1.8	3.6
Outliers	None	None

† Asymmetric unit. ‡ Estimated overall coordinate error based on maximum likelihood.

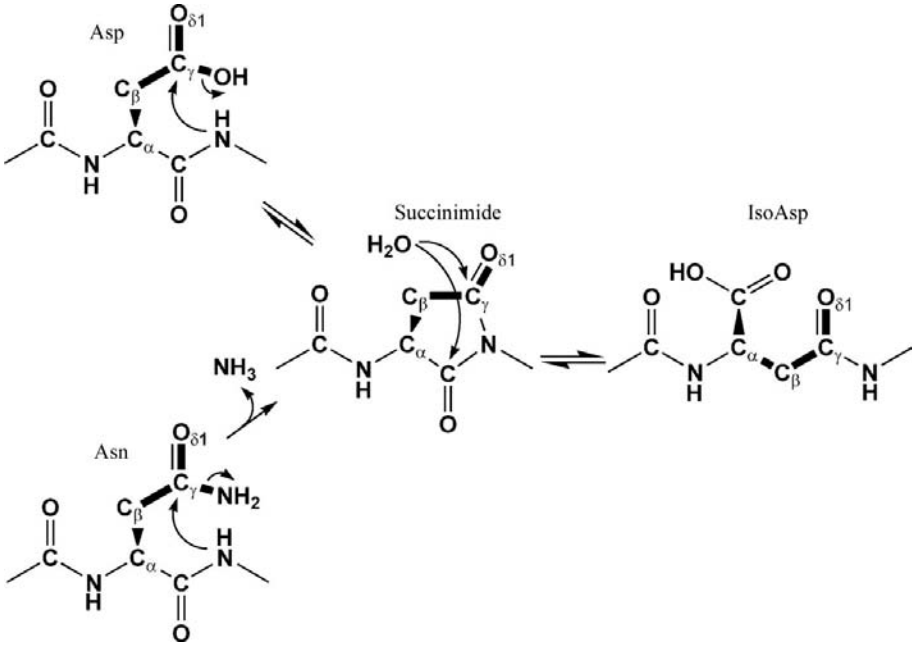

Figure 1
Isomerization of aspartate and deamidation of asparagine. The bonds in the side chains are drawn with bold lines. Note that succinimide can racemize through keto–enol tautomerism.

mice experienced growth retardation and succumbed to fatal seizures, suggesting that the accumulation of damaged proteins is fatal. In some proteins, however, isoAsp formation is thought to be involved in specific *in vivo* processes: for example, in Bcl-x_L (Zhao *et al.*, 2007), ribosomal S11 (David *et al.*, 1999) and MurA (Eschenburg & Schönbrunn, 2000).

The rates of isomerization of Asp and deamidation of Asn depend strongly on the amino-acid sequence, especially on the C-terminal side of Asx residues (where Asx is Asp or Asn). In peptides, the rates are fast for Asx-Gly or Asx-Ser sequences and are slower by one to two orders of magnitude when the side chain on the C-terminal side of Asx is bulkier, such as Val or Leu (Stephenson & Clarke, 1989; Oliyai & Borchardt, 1994). In proteins, isoAsps are generally formed within the labile sequences Asx-Gly or Asx-Ser, but isoAsp formation also occurs within other sequences (Wright, 1991; Johnson & Aswad, 1995; Fujii, Ishibashi *et al.*, 1994; Fujii, Satoh *et al.*, 1994), indicating that the local structure of the protein may assist in isoAsp formation.

The first crystal structure of a protein containing isoAsp was that of purine-specific ribonuclease (RNase) U2 (EC 3.1.27.4; Arima *et al.*, 1968), a member of the RNase T1 family secreted by the smut fungus *Ustilago sphaerogena*, in which isoAsp is formed at Asp45-Glu46 during long crystallization times in acidic solution at pH 4.5 (Noguchi *et al.*, 1995). Among the RNase T1 family proteins, the formation of isoAsp has only been reported in RNase U2. As the structure of RNase U2 with a normal Asp45 sequence is unknown, it remains unclear how the isomerization proceeds at Asp45-Glu46. We have solved the crystal structures of RNase U2 with normal Asp45 (RNase U2A) in complex with adenosine 3′-monophosphate (3′-AMP) at 0.96 and 0.99 Å resolution and discuss here the mechanism of isoAsp formation based on the three-dimensional structures. The mechanism of purine-base recognition by RNase U2 is also discussed.

2. Materials and methods

2.1. Protein preparation and crystallization

RNase U2A was purified from the culture broth of *U. sphaerogena* using anion-exchange and 5′-adenylate-aminohexyl Sepharose affinity chromatography (Uchida & Shibata, 1981). The crystals were grown by the hanging-drop vapour-diffusion method under modified conditions as described previously (Noguchi *et al.*, 1996). 5 µl protein solution containing 20 mg ml^{-1} RNase U2A and 8 m*M* adenosine 3′-monophosphate, adjusted to pH 4.5 with NaOH, was mixed with an equal volume of reservoir solution containing 12.5%(*w*/*w*) polyethylene glycol 8000,

200 m*M* calcium acetate, 100 m*M* sodium cacodylate adjusted to pH 3.75 with a final concentration of 240 m*M* HCl. The mixture was equilibrated against 400 µl reservoir solution at 293 K. In this crystallization condition, two types of crystals were obtained: type VIII and type IX crystals. Both types of crystal were of a thin plate shape, appeared within 3 d and grew to maximum dimensions of approximately 0.30 × 0.30 × 0.05 mm within a week. The crystal parameters are summarized in Table 1, together with the statistics of the X-ray diffraction data collection and crystallographic refinement.

2.2. X-ray diffraction data collection, structure determination and refinement

The crystals were cryoprotected by soaking them in reservoir solution containing 20%(*v*/*v*) polyethylene glycol 400 for a few seconds and were flash-frozen in a stream of N_2 at 95 K just prior to X-ray diffraction data collection. Data collection was performed on beamline 6A at the Photon Factory (Tsukuba, Japan). Diffraction images were processed with the *HKL*-2000 package (Otwinowski & Minor, 1997).

Both crystal structures were determined by the molecular-replacement method using *MOLREP* as implemented in the *CCP*4 package (Collaborative Computational Project, Number 4, 1994) with the type II crystal structure of RNase U2 with isoAsp45 (PDB code 1rtu; Noguchi *et al.*, 1995) as a search model. Crystallographic refinement was performed by *REFMAC*5 (Murshudov *et al.*, 1997) with its default dictionary files, alternating with manual revision of the model using *Coot* (Emsley & Cowtan, 2004). The atomic displacement parameters (*B* factors) of the individual atoms were refined

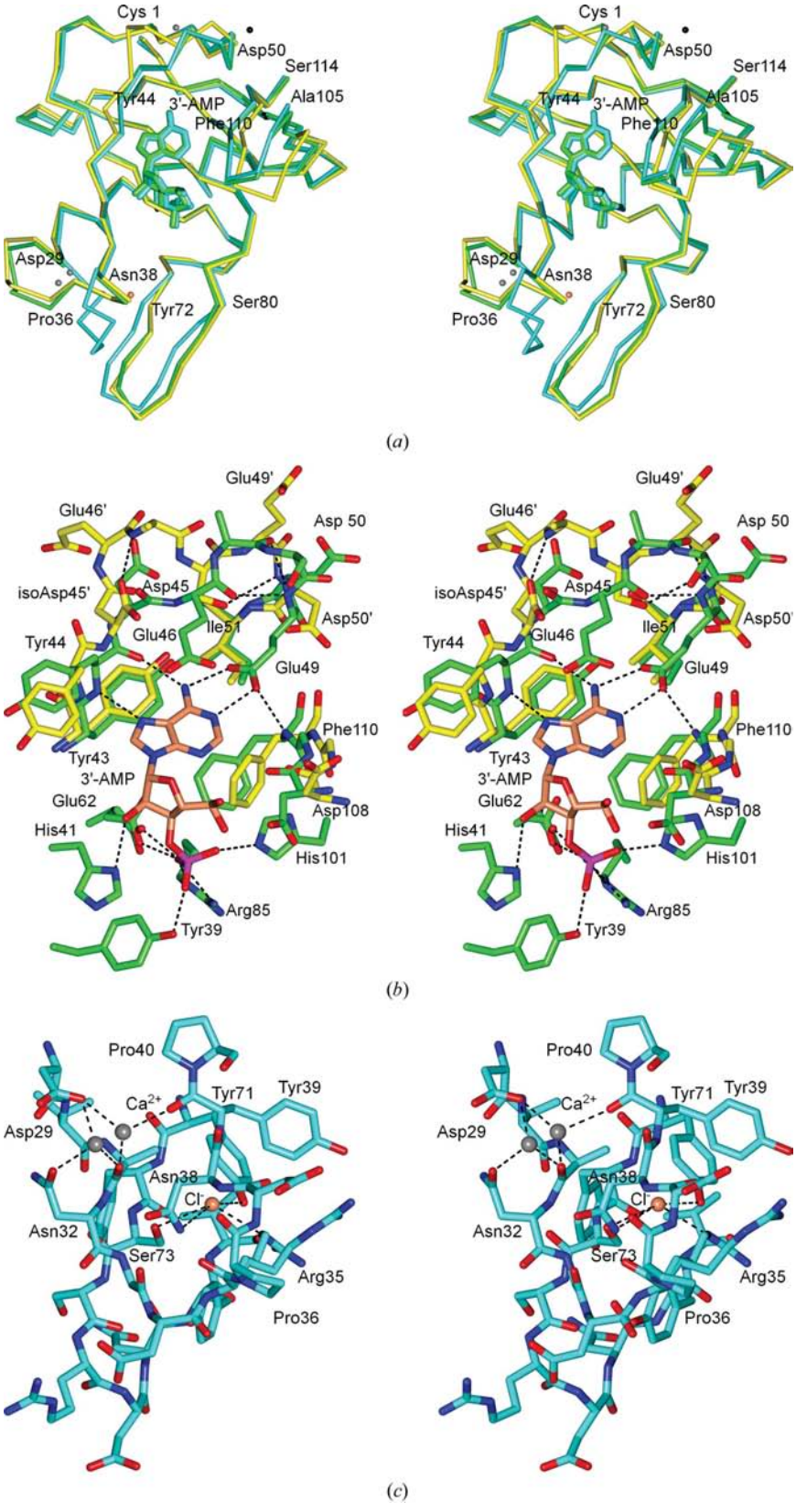

Figure 2
(*a*) Stereoview of the C^{α} traces of the type II (yellow), VIII (green) and IX (cyan) crystal structures, which are superimposed using main-chain atoms in the secondary structures. The bound 3′-AMP molecules are shown as stick models. The calcium ions in the type VIII and IX crystal structures are shown as black and grey spheres, respectively, and the chloride ion in the type IX crystal structure is shown as an orange sphere. (*b*) The stick models around Asp45 and isoAsp45 in the type VIII and II crystal structures. 3′-AMP and the catalytic site residues of the type VIII crystal structure are also shown. The C atoms of RNase U2A in the type VIII and II crystal structures are shown in green and yellow, the C atoms of 3′-AMP are shown in orange and N, O and P atoms are shown in blue, red and magenta, respectively. Hydrogen bonds are drawn as black dotted lines. Residue numbers of the type II crystal structure are indicated with primes. (*c*) The chloride and the calcium ions bound to RNase U2 in the type IX crystal structure. C, N and O atoms are shown in cyan, blue and red, respectively.

anisotropically after the resolution of the refinement was extended to 1.2 Å. H atoms generated at their riding positions were included in the model after the resolution was extended to 1.0 Å. The occupancies of the multiple conformers were determined so that their average *B* factors became comparable. Calcium ions were found in the type VIII and IX crystal structures and chloride ion was found in the type IX crystal structure. The *B* factors of these ions were converged to values that were comparable to those of the protein or solvent atoms around them. In the Bijvoet difference Fourier map, peaks larger than at least 4σ above the average, where σ is the standard deviation, were observed at all positions of ions, S atoms and P atoms. The quality of the refined models was assessed by *PROCHECK* (Laskowski *et al.*, 1993) and *RAMPAGE* (Lovell *et al.*, 2003).

3. Results

3.1. Overall structures

The type II, VIII and IX crystal structures superposed well and structural differences are localized in the regions Asp29–Asn38, Tyr44–Asp50, Tyr72–Ser80 and Ala105–Asp108 (Fig. 2*a*). The structural difference in the region Tyr44–Asp50 is ascribable to isoAsp45 formation in the type II crystal structure. The Glu46–Asp50 regions in the types VIII and IX crystal structures form 3_{10}-helices and the side chains of Glu46 and Glu49 extend toward the bound adenine base of 3′-AMP (Fig. 2*b*). Glu49 $O^{\varepsilon2}$ and Phe110 N form hydrogen bonds with distances of 2.89 Å in the type VIII and 2.88 Å in the type IX crystal structures. In contrast, no hydrogen bond is formed between the main-chain atoms in this region of the type II crystal structure; the carboxyl moieties of Glu46 and Glu49 are located more than 10 Å away from the bound adenine base and the hydrophobic side chains of Ile51, Tyr43 and Phe110 are more exposed to the surface of the protein. The hydrogen bond between Glu49 $O^{\varepsilon2}$ and Phe110 N is lost in the type II crystal structure and this might explain why the region Ala105–Phe110 shifts approximately 1.5 Å away from the adenine-binding site in the type II crystal structure compared with the type VIII and IX crystal structures.

Compared with the type II and VIII crystal structures, one turn of the α-helix from Asp29 to Asn32 in the type IX crystal structure is unfolded and the region Tyr72–Ser80 is shifted approximately 3 Å toward the unfolded region. Pro36, which is buried inside the protein molecule in the type II and VIII crystal structures, is exposed to the solvent region and a chloride ion is located near the position occupied by Pro36 in the type II and VIII crystal structures. The chloride ion is surrounded by the hydrophobic side chains of Tyr39, Tyr78 and Ala31 and forms hydrogen bonds and electrostatic interaction with the side chains of Ser73, Tyr71 and Arg35 (Fig. 2*c*). Calcium ions with partial occupancies are located near the C-terminus of the shortened α-helix in the type IX crystal structure and are coordinated by the O atoms of the unfolded region from Asp29 to Ala33 and the main-chain O atom of Tyr39. The interactions between the bound ions and the protein atoms would stabilize the conformation of this unfolded region in the type IX crystal structure.

3.2. Interaction between 3′-AMP and RNase U2

In the type VIII and IX crystal structures 3′-AMP is defined by clear electron density. Although conformational differences in the region Asp29–Asn38 are observed between the type VIII and IX crystal structures, the interactions between 3′-AMP and RNase U2A are common. Therefore, we will mainly describe the interactions observed in the type VIII crystal structure. The bound 3′-AMP adopts a *syn* conformation about the glycosidic bond and a $C_{3'}$-*endo* sugar pucker (Fig. 2*b*). The phosphate moiety of 3′-AMP is hydrogen bonded to the catalytic site residues of Glu62, His101, Arg85 and Tyr39, which are widely conserved in RNase T1 family proteins (Yoshida, 2001). Two conformers are observed for the side chain of Glu62 and both conformers are hydrogen bonded to the same O3P atom of the phosphate moiety of 3′-AMP. We could not determine the protonation state of Glu62 from the electron-density map owing to this disorder (Ahmed *et al.*, 2007). His41, which is a conserved residue in RNase T1 family proteins, is located near the phosphate moiety and its $N^{\delta1}$ atom is hydrogen bonded to the ribose $O_{2'}$.

The adenine base is located on the hydrophobic surface formed by the aromatic

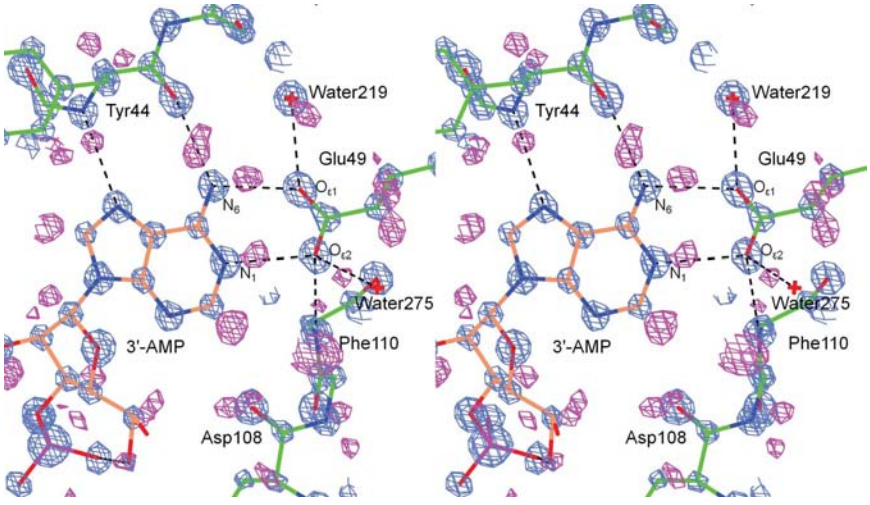

Figure 3
The electron-density maps around Glu49 in the type VIII crystal structure. The map coloured light blue is the σ_A-weighted electron-density map contoured at 4.6σ. The map coloured magenta is the difference Fourier map calculated using the model refined without H atoms and is contoured at 2.2σ. C atoms of RNase U2A and 3′-AMP are shown in green and orange and N, O and P atoms are shown in in blue, red and magenta, respectively. Hydrogen bonds are drawn as black dotted lines.

side chains of Phe110 and Tyr43 and forms four hydrogen bonds to the main-chain atoms of Tyr44 and the side-chain carboxyl moiety of Glu49. In the difference Fourier map calculated with the model refined without H atoms, electron density for the H atom bound to Glu49 $O^{\varepsilon2}$ is observed, as shown in Fig. 3. In the σ_A-weighted electron-density map the $C^{\delta}-O^{\varepsilon1}$ bond of Glu49 shows continuous density, whereas the $C^{\delta}-O^{\varepsilon2}$ bond shows discontinuous density. These clearly indicate that Glu49 $O^{\varepsilon2}$ is protonated. Thus, the $O^{\varepsilon1}$ and $O^{\varepsilon2}$ atoms of the Glu49 side chain are hydrogen bonded as proton acceptors to adenine N_7 and N_2, respectively. Glu49 $O^{\varepsilon2}$ is also hydrogen bonded as a proton acceptor to Phe110 N and as a proton donor to water 275 in a tetrahedral geometry.

3.3. Structure around Asp45

Asp45 is located just beside the adenine-binding site. The σ_A-weighted electron-density maps clearly indicate that Asp45 is not isomerized in the type VIII and IX crystal structures (Figs. 4*a* and 4*b*). Both types of crystals appeared within 3 d. During this period RNase U2A may be dominant in the crystallization droplets, whereas the proportion of RNase U2 with isoAsp45 may still be low. This would explain why only crystals of RNase U2A were obtained. The maps also show continuous and discontinuous electron densities for the $C^{\gamma}-O^{\delta1}$ and $C^{\gamma}-O^{\delta2}$ bonds of Asp45, respectively, indicating that Asp45 $O^{\delta2}$ is protonated. In the type VIII crystal structure, three water molecules, waters 190, 219 and 220, are located near the side chain of Asp45 and form a hydrogen-bond network with the region Tyr43–Glu46 and Ile51 (Fig. 4*c*). The planar carboxyl moiety of Asp45 faces towards Glu46 N and the distance between Asp45 C^{γ} and Glu46 N is 3.50 Å. The Asp45 side-chain conformation is stabilized by the hydrogen bond between Asp45 $O^{\delta1}$ and water 190. The water-mediated hydrogen-bond network and the side-chain conformation of Asp45 are common to the type VIII and IX crystal structures. In the type IX crystal structure a calcium ion is also located near Asp45, and Asp45 $O^{\delta1}$ and Ile51 O are coordinated to the ion. The distance between Asp45 C^{γ} and Glu46 N in the type IX crystal structure is 3.28 Å.

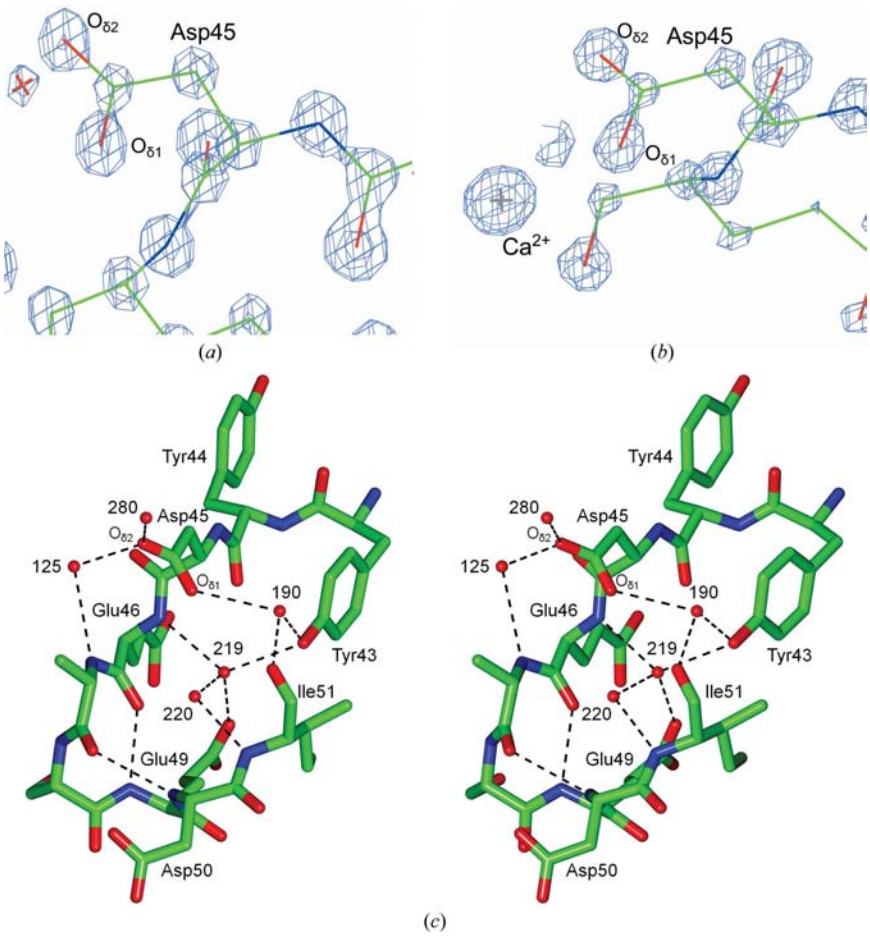

Figure 4
(*a*) σ_A-Weighted electron-density map at Asp45 in the type VIII crystal structure contoured at 3.6σ and (*b*) that in the type XI crystal structure contoured at 4.1σ. The colouring of the maps and the models are the same as in Fig. 3. (*c*) Stereoview of the structure around Asp45 in the type VIII crystal structure. For clarity, water molecules are labelled with their residue numbers only.

4. Discussion

The initial step in the isomerization of Asp45 to isoAsp occurs *via* nucleophilic attack of Glu46 N on Asp45 C^{γ} to form succinimide. The conformation of Asp45-Glu46, in which Asp45 C^{γ} is located just beside Glu46 N, is very suitable for the nucleophilic attack reaction. Water molecules located near Asp45 seem to promote the isomerization reaction. Water 190, which is hydrogen bonded to Asp45 $O^{\delta1}$ as a hydrogen donor, would not only stabilize the Asp45 side-chain conformation suitable for the reaction but would also enhance the electrophilicity of Asp45 C^{γ}. Water 219, which is hydrogen bonded to Glu46 N as a hydrogen acceptor, may enhance the nucleophilicity of Glu46 N. We suppose that the isomerization of Asp45 to isoAsp proceeds as follows. Nucleophilic attack of Glu49 N on Asp45 C^{γ} forms a tetrahedral intermediate (Fig. 5). Water 219 receives a proton from Glu49 N as a general base and water 190 and possibly water 220 stabilize the tetrahedral intermediate through hydrogen-bond formation as proton donors to the $O^{\delta1}$ atom of the tetrahedral intermediate. The $O^{\delta2}$ atom of the intermediate receives a proton from water 125 or water 280 and leaves the C^{γ} atom, resulting in succinimide formation. In the next step, a water molecule from the bulk-solvent region initiates a nucleophilic attack on the C atom

derived from the main-chain carbonyl C atom of Asp45 to hydrolyze the succinimide. Water 219 as a general acid provides a proton for the leaving Glu46 N and isoaspartate is formed. Isoaspartate formation may induce a conformational change in the region Tyr44–Asp50, as in the type II crystal structure. In the type II crystal structure, water 330 is hydrogen bonded to Ile51 O, Tyr43 O^{η} and isoAsp45 $O^{\delta1}$ and the hydrogen-bonding scheme of this water molecule is identical to that of water 190 in the type VIII and IX crystal structures, since isoAsp45 $O^{\delta1}$ is derived from Asp45 $O^{\delta1}$. This suggests that the water 190 occupies the same position throughout the isomerization reaction.

The conformation of the region Tyr43–Ile51, which is suitable for the isomerization of Asp45, is stabilized by intramolecular hydrogen bonds in the 3_{10}-helix from Glu46 to Asp49 and by the water-mediated hydrogen-bond network as shown in Fig. 4(*b*). Owing to these hydrogen bonds, the conformations of the region in the presence and absence of the bound 3′-AMP would differ little from each other. Therefore, the isomerization of Asp45 is presumed to proceed regardless of the presence of bound 3′-AMP.

Comparison of RNase U2 crystal structures demonstrates that isoAsp formation rearranges the locations of the charged side chains of the region Asp45–Asp50 and causes the exposure of the hydrophobic side chains near the adenine-binding site. These would alter the surface properties of the protein. Although data for the enzymatic activity is not reported, RNase U2 with isoAsp45 is thought to lose the ability to recognize the base of the RNA substrate because the side chain of Glu49, which is the key residue for base recognition, is located away from the adenine-binding site. This suggests that the structural changes caused by isoAsp formation would alter the solubility or stability of proteins and impair their function and that the accumulation of proteins containing isoAsp in cells might cause aggregation of the proteins or cause dysfunction of the cells. It is plausible that the accumulation of protein with isoAsp is related to the progression of disease or the aging process.

A conformational difference at Asp29–Asn38 is observed between the type VIII and IX crystal structures, even though the crystals were grown under identical solution conditions. This suggests that the region is very flexible and that the C-terminal region of the α-helix, Asp29–Asn32, is in equilibrium between α-helical and unfolded conformations in solution. Asn32 is reported to be easily deamidated and isomerized to isoaspartate *via* succinimide by alkaline treat-

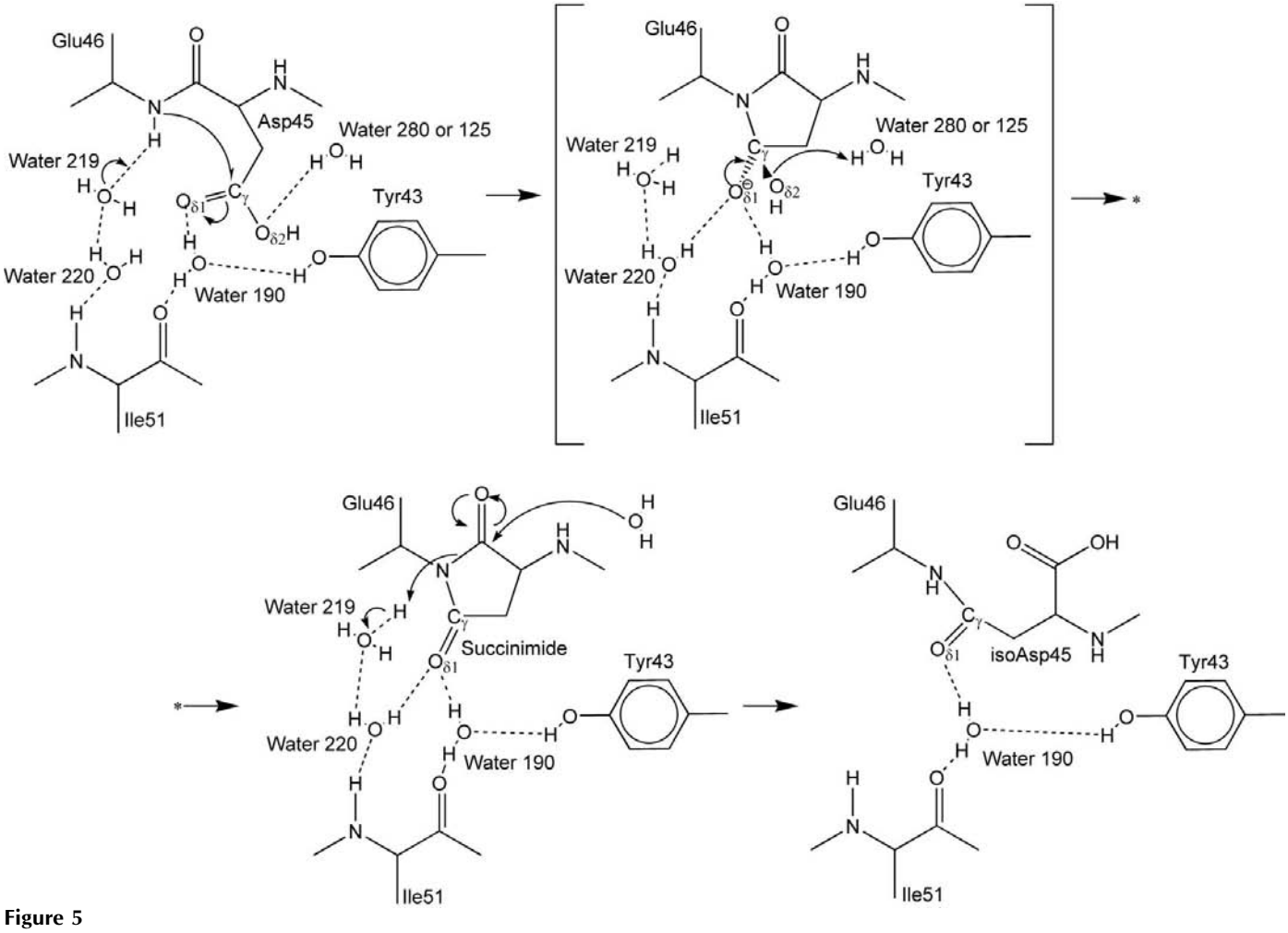

Figure 5
Proposed reaction mechanism of the isomerization of Asp45.

ment (Kanaya & Uchida, 1986). It is difficult for Asn32-Gly33 in an α-helical conformation to form succinimide because the conformation hinders the nucleophilic attack of Gly33 N on Asn32 C^{γ}. Thus, deamidation would only proceed when the C-terminal region of the helix is unfolded. The α-helix content of RNase U2 decreases when isoAsp32 is formed as determined from CD spectra (Uchida & Shibata, 1981), suggesting that the region Asp29–isoAsp32 can no longer form an α-helix.

RNase U2 recognizes adenine and guanine bases of single-stranded RNA: the K_m values for adenylyl-3′,5′-cytidine and guanylyl-3′,5′-cytidine are 450 and 530 μM, respectively (Uchida & Machida, 1978). When the guanine base is placed at the adenine-binding site of the type VIII crystal structure so that the purine rings are superimposed, two close contacts are observed between Tyr44 O and guanine O_6 at 2.8 Å and between Asp108 O and guanine N_2 at 2.0 Å. The former contact could be removed by a small reorientation of the peptide bond between Tyr44 and Asp45 or possibly by a peptide-bond flip to form a hydrogen bond between Asp45 N and guanine O_6. As the region Ala105–Phe110 is suggested to be able to shift so as to widen the adenine-binding site as described above, the latter contact would also be removed by the shift; moreover, hydrogen-bond formation between Asp108 O and guanine N_7 is possible. Glu49 would be able to form two hydrogen bonds as observed in the type VIII and IX crystal structures when Glu49 $O^{\varepsilon 1}$ is protonated instead of Glu49 $O^{\varepsilon 2}$: the protonated Glu49 $O^{\varepsilon 1}$ acts as a hydrogen donor to guanine O_6 and Glu49 $O^{\varepsilon 2}$ acts as a hydrogen acceptor to guanine N_1. Alternatively, Glu49 $O^{\varepsilon 1}$ and $O^{\varepsilon 2}$ as hydrogen acceptors could form hydrogen bonds to guanine N_1 and N_2, respectively, as observed in the case of guanine-specific RNase T1 (Heinemann & Han, 1989), since the Glu49 side chain is less restrained by van der Waals contacts with the protein atoms and a small shift of its carboxyl moiety is possible. These observations suggest that the adenine-binding site of RNase U2 could also accommodate a guanine base.

This work was supported by Grant-in-Aids for Scientific Research to SN (No. 07772128) from the Ministry of Education, Science, Sports and Culture, Japan. The synchrotron-radiation experiments were performed under the approval of the Photon Factory Program Advisory Committee (Proposal No. 2008G141).

References

Ahmed, H. U., Blakeley, M. P., Cianci, M., Cruickshank, D. W. J., Hubbard, J. A. & Helliwell, J. R. (2007). *Acta Cryst.* D**63**, 906–922.
Arima, T., Uchida, T. & Egami, F. (1968). *Biochem. J.* **106**, 601–607.
Aritomi, M., Kunishima, N., Inohara, N., Ishibashi, Y., Ohta, S. & Morikawa, K. (1997). *J. Biol. Chem.* **272**, 27886–27892.
Cacia, J., Keck, R., Presta, L. G. & Frenz, J. (1996). *Biochemistry*, **35**, 1897–1903.
Clarke, S. (1993). *Curr. Opin. Cell Biol.* **5**, 977–983.
Collaborative Computational Project, Number 4 (1994). *Acta Cryst.* D**50**, 760–763.
David, C. L., Keener, J. & Aswad, D. W. (1999). *J. Bacteriol.* **181**, 2872–2877.
Dick, L. W. Jr, Qiu, D. & Cheng, K.-C. (2009). *J. Chromatogr. B*, **877**, 3841–3849.
Emsley, P. & Cowtan, K. (2004). *Acta Cryst.* D**60**, 2126–2132.
Eschenburg, S. & Schönbrunn, E. (2000). *Proteins*, **40**, 290–298.
Fujii, N., Ishibashi, Y., Satoh, K., Fujino, M. & Harada, K. (1994). *Biochim. Biophys. Acta*, **1204**, 157–163.
Fujii, N., Satoh, K., Harada, K. & Ishibashi, Y. (1994). *J. Biochem.* **116**, 663–669.
Heinemann, U. & Han, U. (1989). *Protein–Nucleic Acid Interaction*, edited by W. Saenger & U. Heinemann, pp. 111–141. London: Macmillan.
Johnson, B. A. & Aswad, D. W. (1995). *Deamidation and Isoaspartate Formation in Peptides and Proteins*, edited by D. W. Aswad, pp. 91–113. Boca Raton: CRC Press.
Kanaya, S. & Uchida, T. (1986). *Biochem. J.* **240**, 163–170.
Kim, E., Lowenson, J. D., MacLaren, D. C., Clarke, S. & Young, S. G. (1997). *Proc. Natl Acad. Sci. USA*, **94**, 6132–6137.
Laskowski, R. A., MacArthur, M. W., Moss, D. S. & Thornton, J. M. (1993). *J. Appl. Cryst.* **26**, 283–291.
Lovell, S. C., Davis, I. W., Arendall, W. B. III, de Bakker, P. I. W., Word, J. M., Prisant, M. G., Richardson, J. S. & Richardson, D. C. (2003). *Proteins*, **50**, 437–450.
Murshudov, G. N., Vagin, A. A. & Dodson, E. J. (1997). *Acta Cryst.* D**53**, 240–255.
Noguchi, S., Satow, Y., Uchida, U., Sasaki, C. & Matsuzaki, T. (1995). *Biochemistry*, **34**, 15583–15591.
Noguchi, S., Satow, Y., Uchida, U., Sasaki, C. & Matsuzaki, T. (1996). *J. Cryst. Growth*, **168**, 270–274.
Oliyai, C. & Borchardt, R. T. (1994). *Pharm. Res.* **11**, 751–758.
Otwinowski, Z. & Minor, W. (1997). *Methods Enzymol.* **276**, 344–358.
Potter, S. M., Henzel, W. J. & Aswad, D. W. (1993). *Protein Sci.* **2**, 1648–1663.
Roher, A. E., Lowenson, J. D., Clarke, S., Wolkow, C., Wang, R., Cotter, R. J., Reardon, I. M., Zurcher-Neely, H. A., Heinrikson, R. L., Ball, M. J. & Greenberg, B. D. (1993). *J. Biol. Chem.* **268**, 3072–3083.
Stephenson, R. C. & Clarke, S. (1989). *J. Biol. Chem.* **264**, 6164–6170.
Uchida, T. & Machida, C. (1978). *Nucleic Acids Res.* **5**, s409–s412.
Uchida, T. & Shibata, Y. (1981). *J. Biochem.* **90**, 463–471.
Weber, D. J., McFadden, P. N. & Caughey, B. (1998). *Biochem. Biophys. Res. Commun.* **246**, 606–608.
Wright, H. T. (1991). *Protein Eng.* **4**, 283–294.
Yoshida, H. (2001). *Methods Enzymol.* **341**, 28–41.
Zhang, W., Czupryn, M. J., Boyle, P. T. Jr & Amari, J. (2002). *Pharm. Res.* **19**, 1223–1231.
Zhao, R., Oxley, D., Smith, T. S., Follows, G. A., Green, A. R. & Alexander, D. R. (2007). *PLoS Biol.* **5**, 39–53.